Spatial and temporal aspects of neuronal calcium and sodium signals measured with low-affinity fluorescent indicators

Marco Canepari, William Ross

Spatial and temporal aspects of neuronal calcium and sodium signals measured with low-affinity fluorescent indicators

Marco Canepari[1,2,3,*], **William N Ross**[4]

[1]Univ. Grenoble Alpes, CNRS, LIPhy, F-38000 Grenoble, France. [2]Laboratories of Excellence, Ion Channel Science and Therapeutics, Valbonne, France. [3]Institut National de la Santé et Recherche Médicale, Paris, France. [4]Department of Physiology, New York Medical College, Valhalla, NY 10595, USA.

***Address of the submitting and corresponding author:** Marco Canepari, Laboratoire Interdisciplinaire de Physique (UMR 5588), Bat. E45, 140 avenue de la physique, Domaine univ., 38402 St Martin d'Hères cedex, France. Email: marco.canepari@univ-grenoble-alpes.fr

Acknowledgements: This work was supported for MC by the *Agence Nationale de la Recherche* through the Labex *Ion Channels Science and Therapeutics* (program number ANR-11-LABX-0015) and for WNR by the National Institute of Health (grant R01NS099122) and by the US-Israel Binational Science Foundation (Grant No: 2017163).

Conflict of interest statement: *The authors declare no conflicts of interest.*

Keywords: Imaging, calcium, sodium, neuron, ion channels, axon, dendrite, spine.

Abstract

Low-affinity fluorescent indicators for Ca^{2+} or Na^{+} allow measuring the dynamics of intracellular concentration of these ions with little perturbation from physiological conditions because they are weak buffers. When using synthetic indicators, which are small molecules with fast kinetics, it is also possible to extract spatial and temporal information on the sources of ion transients, their localization, and their disposition. This review examines these important aspects, from the biophysical point of view, and how they have been recently exploited in neurophysiological studies. We first analyze the environment where Ca^{2+} and Na^{+} indicators are inserted, highlighting the interpretation of the two different signals. Then, we address the information that can be obtained by analyzing the rising phase and the falling phase of the Ca^{2+} and Na^{+} transients evoked by different stimuli, focusing on the kinetics of ionic currents and on the spatial interpretation of these measurements, especially on events in axons and dendritic spines. Finally, we suggest how Ca^{2+} or Na^{+} imaging using low-affinity synthetic fluorescent indicators can be exploited in future fundamental or applied research.

Introduction

In the last decades, optical recordings of intracellular transients of Ca^{2+} [21] and Na^{+} [63] concentrations have been extensively used to investigate neuronal activity. With the notable exception of Ca^{2+} transients mediated by Ca^{2+} release from intracellular stores [9], neuronal Ca^{2+} and Na^{+} signals are mediated by ion influx through the plasma membrane either associated with electrical events or with the activation of receptors. In the first case, the major sources of ion influx are voltage-gated Ca^{2+} channels (VGCCs) and voltage-gated Na^{+} channels (VGNCs), which are members of the voltage-gated ion channel superfamily [78]. The most common examples are the Ca^{2+} and Na^{+} transients associated with action potentials (APs). In the second case, the major sources of ion influx are diverse ligand-gated cation channels with various permeabilities to Ca^{2+} and Na^{+} [58], but other cation channels such as transient receptor potential channels [77] can also contribute to Ca^{2+} and Na^{+} influx. Thus, local Ca^{2+} and Na^{+} transients are often associated with specific neuronal events.

Optical recordings of Ca^{2+} or Na^{+} concentration changes are ultimately indirect measurements of the fluorescence of an indicator, which is a molecule that binds to the ion and changes its photon absorption and emission. While this molecule can be a genetically encoded protein [41], organic indicators are still widely used since they can reveal information that would not be available otherwise [64]. In all cases, the biophysical challenge consists in extracting, from this indirect measurement, the physiologically relevant information. Practical and functional considerations have been addressed in the literature, for instance, to interpret Ca^{2+} imaging data in small neuronal compartments in brain slices [26] or *in vivo* [5]. The ability of Ca^{2+} and Na^{+} recordings to dissect the origin and kinetics of diverse ion channels, as well as the dynamics of the ions and their interaction with the native environment, depends on the spatial and temporal resolution of the imaging techniques utilized in the experiments. Recent work performed in individual neurons in brain slices, filled with ion indicators through somatic patch clamp recordings, exploit the high spatial and temporal resolution of camera imaging to extract quantitative information on ion channels and intracellular processes triggered by ion influx in several neuronal compartments, including synaptic spines [50,51,53,75], neuronal dendrites [1,2,6,30,31,60] and axons [8,19,20,24,36,40,65,73]. The aim of this article is to review the biophysical aspects that were considered in these studies to unravel the native molecular dynamics occurring in neuronal compartments.

Biophysical environment of Ca^{2+} and Na^{+} fluorescence measurements

When loading a neuron with a Ca^{2+} or a Na^{+} indicator, the first element to be considered is the perturbation to the physiological signaling conditions that is caused by the introduction of the exogenous buffer. In the case of Ca^{2+} indicators, a distinction is made between high-affinity and low-affinity indicators [59], the first group having an equilibrium constant (K_D) <1 µM and the second group a K_D > 10 µM. The distinction is normally made with respect to the endogenous Ca^{2+} buffer of the cells that can be highly variable [45]. In the case of Na^{+} indicators [46], there are only two useful compounds, and they have K_Ds in the millimolar range and their buffering is negligible in physiological conditions. Thus, Na^{+} dyes can be always considered low-affinity indicators. If the dye is introduced into the cell at known

concentration by establishing a whole cell patch clamp recording, the electrical activity at the electrode site can be correlated with the ion signal and the total concentration of the indicator is that in the pipette solution after diffusional equilibrium [7].

As shown in the scheme of Fig.1, while the loading procedure is identical for Ca^{2+} and Na^{+} indicators, the biophysical conditions for Ca^{2+} and Na^{+} transients are different. In the case of Ca^{2+}, the concentration gradient of the free ion between the intracellular and the extracellular spaces is several orders of magnitudes, from nominally 0 (<100 nM) in the cytosol to 1-2 mM outside the cell. Indeed, intracellular Ca^{2+} is buffered by diverse Ca^{2+}-binding proteins that determine the endogenous buffering capacity, defined as the ratio between the bound and free Ca^{2+}. The endogenous buffer capacity varies from cell to cell, but also within different compartments of the same cell [45]. In CA1 hippocampal pyramidal neurons, for instance, the endogenous buffering capacity may vary from ~20 in dendritic spines [67] to ~200 in dendritic bulks [25]. In the dendrites of cerebellar Purkinje neurons, it can reach values of ~2000 [16]. Loading a cell with a Ca^{2+} indicator increases the total buffering capacity by a factor that is given by the ratio between the dye concentration and its K_D. For low-affinity Ca^{2+} indicators with K_D = 10-50 µM at concentrations of 0.15-2 mM, the additional buffering capacity may range between 3 and 200, a value that can be either smaller or larger than the endogenous buffering capacity. At this point, the short (1-20 ms) opening of Ca^{2+} channels produces a Ca^{2+} influx that transitorily and locally increases the intracellular total Ca^{2+} concentration to values that typically range between 10 µM to 100 µM, although larger transients can be potentially reached with longer time windows. Of these Ca^{2+} ions, only a very small fraction remains free whereas the rest binds to membrane proteins (immobile buffer), to cytosolic proteins (mobile buffer) and to the dye (Fig.1). Notably, since the total Ca^{2+} influx is normally limited to ≤100 µM, loading the cell with any Ca^{2+} indicator at concentrations ≥500 µM prevents dye saturation since less than 20% of the dye is bound to Ca^{2+} following a Ca^{2+} transient. After a Ca^{2+} transient has reached a maximal value, the initial cytoplasmic Ca^{2+} concentration is eventually restored by extrusion through multiple Ca^{2+} pumps [44].

In the case of Na^{+}, the concentration gradient between the intracellular and the extracellular spaces is of the order of 10, from a few millimolar in the cytosol to >100 mM outside the cell, leading to a smaller driving force for Na^{+} with respect to Ca^{2+}. Commercial Na^{+} indicators SBFI and ANG-2 (or ING-2) have K_D measured in cuvettes of 7.4 mM [46] and 8.3 mM [61] respectively, but higher values were obtained in measurements that were performed in neurons [50,63]. The low affinity of these indicators guarantees that the fluorescence change is linearly related to the change in ion concentration. Thus, only a fraction of Na^{+} is sequestrated by the dye and the concentration of the free dye is always higher than that of the bound dye. Notably, since Na^{+} is either free or bound to dye, the accurate measurement of the fractional change of fluorescence can be translated to quantitative estimates of the bound and free Na^{+} concentrations after correcting for background fluorescence [18]. As an example, in the case of an AP in the axon initial segment (AIS) of the neocortical layer-5 (L5) pyramidal neuron, the transient opening of Na^{+} channels produces local Na^{+} influx that increases the intracellular Na^{+} concentration by 0.7-1.4 mM [18,20,40]. Since only a fraction of this Na^{+} binds to the dye and there is no significant endogenous Na^{+} buffer, the majority of this ion which remains free equilibrates in the cytoplasm by diffusion [20,51,52] and it is finally extruded by Na^{+} pumps to restore the initial condition [35].

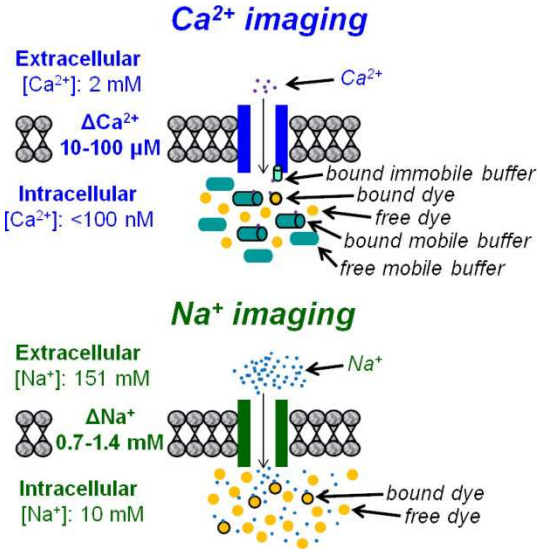

Figure 1. Recording conditions in Ca^{2+} and Na^{+} imaging. The indicated extracellular and intracellular Ca^{2+} and Na^{+} concentrations are those of the solutions used in Canepari's laboratory. In Ca^{2+} recordings (top), Ca^{2+} ions entering the cell bind to the immobile buffer (membrane proteins), to the mobile buffer (cytosolic proteins) and to the dye. Free Ca^{2+} is negligible with respect to bound Ca^{2+}. Free dye is higher than bound dye when using a low-affinity indicator. In Na^{+} recordings (bottom), mM Na^{+} entering the cell (estimated for an AP in the AIS of L5 pyramidal neurons) binds to the dye only. Free Na^{+} and free dye are higher than bound dye.

Spatial and temporal interpretation of Ca^{2+} and Na^{+} fluorescence signals

Considering ion-binding kinetics and diffusion, in addition to the general biophysical conditions described in the previous paragraph, allows the interpretation of the spatial and temporal aspects of Ca^{2+} and Na^{+} fluorescence signals. Fig.2A shows an example of a localized ion source where influx occurs in a small protrusion, which can be, for instance, a synaptic terminal or a dendritic spine. In the case of Ca^{2+}, ions bind to a mobile buffer and indicator and both bound species can diffuse away from the protrusion and equilibrate in the bulk. This means that the presence of the indicator may facilitate Ca^{2+} transport and that a delayed fluorescent transient can be in principle detected outside the protrusion [43,66]. Both phenomena critically depend on the affinity of the indicator. Whereas high-affinity indicators can transport Ca^{2+} for longer distances producing fluorescent transients several microns away from the cell membrane [12], Ca^{2+} bound to low-affinity indicators equilibrates with unbound buffers close to the source and signals can be localized in small domains [13]. In the case of Na^{+}, in contrast, most ions remain free and rapidly diffuse outside the protrusion [20,50]. This means that fluorescent transients rapidly decay from the localized source and fluorescence signals can be detected at the adjacent sites of the bulk cytoplasm. The spatial uniformity of the ion source, together with the kinetics of diffusion, have important consequences when analyzing the time course of fluorescence signals, as illustrated in Fig.2B. In the case of Ca^{2+}, whereas the K_{ON} of the dye is very fast, being limited only by diffusion of this relatively small molecule [34], the cooperative binding to mobile proteins such as parvalbumin [39], calbindin [54] and calretinin [15] is governed by complex kinetics leading to slower equilibration. Thus, on a fast time scale, Ca^{2+} can initially bind to dye and afterwards can be sequestered by an endogenous protein. This mechanism, which is responsible for fast decay of the fluorescence signal in cerebellar Purkinje neurons following the activation of the climbing fiber [47], can occur also when Ca^{2+} influx is spatially uniform. In the case of Na^{+}, in contrast, the concentration of the free ion equilibrates very rapidly in space with a diffusion coefficient <1 $\mu m^2 \cdot ms^{-1}$ [38], potentially leading to fast decay of fluorescence signals at the site of initial Na^{+} accumulation if Na^{+} influx is not spatially uniform [18,20,40,50,52,73]. The two processes of Ca^{2+} sequestration and Na^{+} diffusion, which depend on the biochemical composition of the endogenous Ca^{2+} buffer and on the spatial organization of the ion sources respectively, are

responsible for the early part of the falling phase of the ion fluorescence signals. The time scale of these two mechanisms may overlap with the time window of ion entry. In the second case, i.e. when the time-window of ion influx precedes the mechanisms responsible for ion decay, the kinetics of the rising phase of the fluorescence signal and that of the ionic current are linearly correlated when the indicator is far from being saturated. Thus, the time course of the fluorescence signal is linear with the integral of the ion influx in the time scale of the equilibration of the ion-dye binding reaction. In the opposite case, i.e. when the buffer-dye sequestration processes for Ca^{2+} or the spatial equilibration of Na^{+} (see [73]) begin in the time-window of the ion influx, the linearity between the rising phase of the fluorescence signal and the ionic current is compromised. Fig.2C shows the time-course of fluorescence signals obtained from computer simulations using the algorithms reported in [3]. If Ca^{2+} sequestration or Na^{+} diffusion are neglected, the time-derivative of the fluorescence signals match the kinetics of the Ca^{2+} or the Na^{+} current. In contrast, if Ca^{2+} sequestration or Na^{+} diffusion are not negligible, the resulting fast decay of the fluorescence signals leads to negative components of the respective time-derivatives that consequently do not match the kinetics of the Ca^{2+} or Na^{+} current.

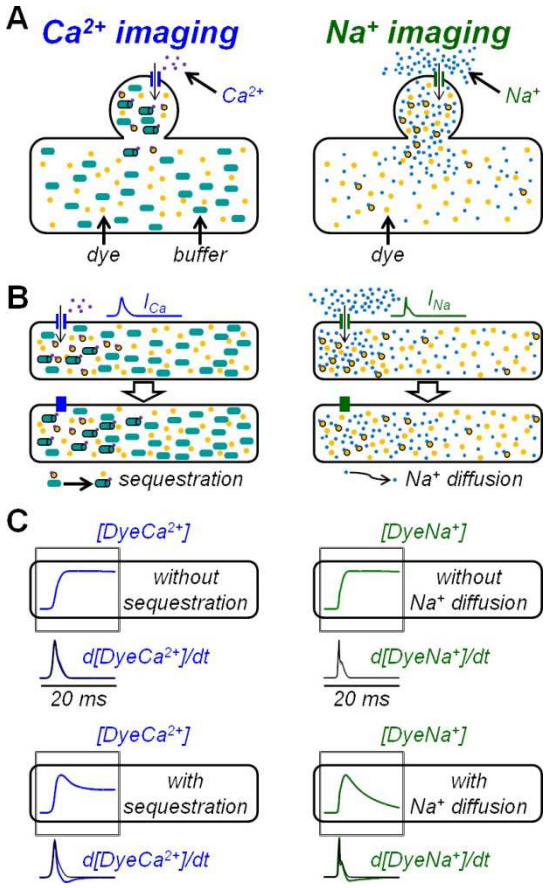

Figure 2. Spatial and temporal development of Ca^{2+} and Na^{+} fluorescence signals. **(A)** Spatial development of ion signals generated at a protrusion. In Ca^{2+} recordings (left), Ca^{2+}-bound mobile buffer and dye can diffuse outside the protrusion and equilibrate in the bulk. In Na^{+} recordings (right), free and dye-bound Na^{+} can diffuse outside the protrusion and equilibrate in the bulk. **(B)** Temporal development of ion signals. In Ca^{2+} recordings (left), intracellular Ca^{2+} elevated by the current I_{Ca} binds to dye and mobile buffer with different kinetics: Ca^{2+} initially bound to dye (top) is later sequestrated by buffer (bottom). In Na^{+} recordings (right), intracellular Na^{+} elevated by the current I_{Na} partially binds to dye (top) and later both free and bound Na^{+} diffuse away from the site of influx (bottom). **(C)** With respect to the scenarios in panel B, comparison between the kinetics of the currents (superimposed black traces) and those of the time-derivatives of dye-bound transients from computer simulations. Top, in the absence of Ca^{2+} sequestration from dye to buffer (left), or Na^{+} diffusion (right), time-derivatives match currents. Bottom, with Ca^{2+} sequestration (left), or Na^{+} diffusion (right), time-derivatives don't match currents.

The rising phase of Ca^{2+} and Na^{+} signals and the derivation of ionic currents in dendrites and axons

From the considerations reported in the previous paragraph it follows that Ca^{2+} and Na^{+} signals are characterized by two temporal phases: (1) a rising phase dominated by the ion influx and (2) a falling phase dominated by diffusion, buffer sequestration and extrusion. The mechanisms underlying the two phases generally overlap and the end of the rising phase normally coincides with the beginning of the

falling phase. In several cases, however, the end of the rising phase is characterized by the appearance of a brief plateau. Under this condition, the temporal overlap can be considered small enough to be neglected so that the slope of the early part of the rising phase of the signal is entirely governed by ion influx. In these cases, the kinetics of the ionic current can be extrapolated from the signal with temporal precision given by the relaxation time of the dye-ion reaction.

Conventionally, ionic currents are measured using the patch clamp technique in voltage clamp mode [70], an approach that consists of maintaining the membrane potential (V_m) at the tip of an electrode at given values by injecting currents and then at measuring the additional current necessary to clamp the V_m when ion channels open or close. This approach is ideal for recording ionic currents from ion channels expressed in electrically uniform host systems [23], but it fails in native systems where the V_m is not uniform. In these cells, the kinetics of Ca^{2+} and Na^+ currents at their sites of origin can be in principle derived from the analysis of the rising phase of fluorescence signals independently of the V_m, i.e. without artificially clamping the V_m at the site of the electrode. This quantitative approach was initially pioneered by Ogden et al. [57] and by Sabatini and Regehr [68] who estimated the kinetics of Ca^{2+} currents obtained in the axons of cerebellar granule cells using the time-derivative of fluorescence transients. The formal procedure to extrapolate the kinetics of the Ca^{2+} current was further developed by Jaafari et al. [32] in experiments on the apical dendrites of CA1 hippocampal pyramidal neurons from brain slices. Cells were filled with relatively high concentrations (1-2 mM) of the low-affinity Ca^{2+} indicator Oregon Green BAPTA-5N to obtain enough resting fluorescence when sampling at 20 kHz. In this preparation, as shown in the example of Fig.3A, the fluorescence increase associated with the back-propagating AP (bAP) reaches a plateau that lasts for a few milliseconds after the end of the bAP. In this case, the kinetics of the Ca^{2+} current can be extracted by calculating the time-derivative of the fluorescence transient either filtered by a smoothing algorithm or fitted by a model function to obtain a noise-free estimate of the current [33]. As shown in Fig.3A, the Ca^{2+} current associated with the bAP in the apical dendrite of a pyramidal neuron peaks during the decay phase of the somatic AP, which reflects the delayed activation of VGCCs by the depolarizing waveform. Technically, although the kinetics of the Ca^{2+} current could be sampled at a few kilohertz, the highest possible acquisition rate was desirable in this measurement since the current extraction is the result of the calculation of a time derivative. Thus, the acquisition rate of 20 kHz was necessary to precisely reconstruct the kinetics of the Ca^{2+} currents associated with bAPs along the entire apical dendrite, and to link these currents to the diverse activated VGCCs [31].

The same concept utilized to analyze the rising phase of Ca^{2+} transients applies to Na^+ transients. In this case, however, the discriminating mechanism that separates the rising and the falling phases of the fluorescence transient is the diffusion of free Na^+, as shown in the simulation of Fig.2C. Precisely, the extent to which free Na^+ diffusion affects the Na^+ transient at each individual site depends on the spatial arrangement of the Na^+ influx and on the morphology of cellular compartments. In the case of the AIS of L5 pyramidal neurons, it was shown that the relatively long segment (~40 µm) where VGNCs are clustered and the conical shape of the structure ending in the cell body make the contribution of Na^+ longitudinal diffusion small in the ~1 ms time scale [18], but the scenario is different in a Ranvier node [20]. This is the characteristic time scale of activation and inactivation of VGNCs. Thus, as shown in the

example of Fig.3B, the Na^+ current associated with the generating AP could be extracted by calculating the time-derivative of a fitted fluorescence transient recorded at 10 kHz. Notably, in contrast to the case of the Ca^{2+} current, the Na^+ current could be calibrated in terms of pA/µm^2 after converting the fluorescence change to Na^+ concentration and estimating the surface/volume of the axonal compartment [18]. As shown in the example of Fig.3B, the largest and fastest component of the Na^+ current peaks at the beginning of the rising phase of the somatic AP. This component, which is due to fast inactivating VGNCs [76], is a mark of the kinetics of VGNCs. This approach of extracting the Na^+ current was later utilized to investigate in detail the current components of the two VGNC types expressed in L5 pyramidal neurons, namely $Na_v1.2$ and $Na_v1.6$ [19]. Interestingly, it was found that in the distal part of the AIS the Na^+ current and Ca^{2+} current associated with an AP have similar kinetics since they both peak at the AP upstroke, in contrast to the proximal part of AIS where the kinetics of the two signals are different [36,40]. This phenomenon is due to the Ca^{2+} permeability of $Na_v1.2$ [24], which determines a major component of Ca^{2+} current compared to the slower one mediated by VGCCs. Note, in that study, Na^+ and Ca^{2+} measurements were obtained in separated recordings. Yet, simultaneous Na^+ and Ca^{2+} measurements at high speed are achievable [49], potentially allowing the simultaneous extraction of Na^+ and Ca^{2+} currents.

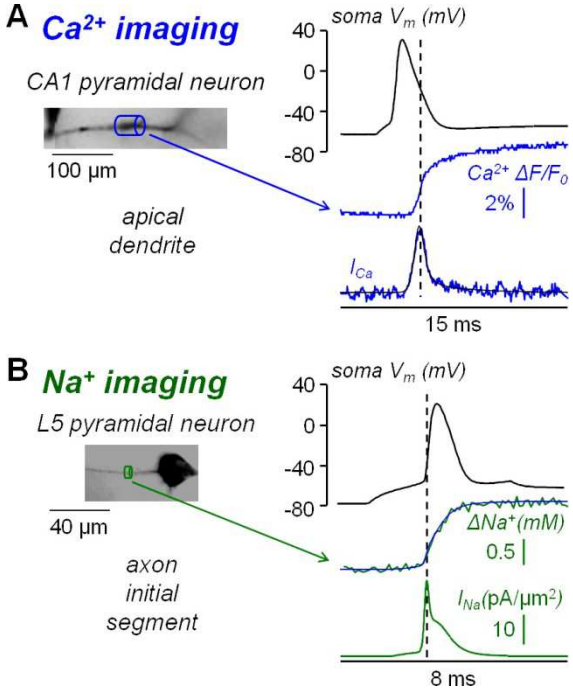

Figure 3. Examples of extraction of Ca^{2+} and Na^+ currents from time-derivatives of fluorescence signals. **(A)** In Ca^{2+} recordings from an apical dendritic region of a CA1 hippocampal pyramidal neuron filled with 2 mM OG5N, the fluorescence transient associated with a bAP is acquired at 20 kHz (average of 9 trials). The time-derivative representing the Ca^{2+} current (I_{Ca}) is calculated either from the smoothed signal (blue trace) or from its fit (black trace superimposed). I_{Ca}, peaking during the somatic AP decay, is not calibrated. **(B)** In Na^+ recordings from a site on the AIS of a L5 pyramidal neuron filled with 0.5 mM ING-2, the fluorescence transient associated with an AP is acquired at 10 kHz (average of 4 trials. The time-derivative representing the Na^+ current (I_{Na}) is calculated from its fit. I_{Na}, peaking at the beginning of the somatic AP upstroke, is calibrated in pA/µm^2 after estimating the diameter of the AIS.

The falling phase of Ca^{2+} and Na^+ signals in dendrites and axons

The falling phase of evoked Ca^{2+} transients using low-affinity indicators varies depending on the cell type and location within the cell. In dendrites and axons, this decay phase is due to a combination of Ca^{2+} binding to endogenous buffers, membrane pumps, and Na^+/Ca^{2+} exchangers. Diffusion of Ca^{2+}, as a removal process, is not important in most cases, mainly because binding of Ca^{2+} to intracellular proteins and membranes slows diffusion by ~100 times compared to diffusion in water [38]. The falling phase of evoked Na^+ transients often appears similar to that of evoked Ca^{2+} signals, but the underlying

mechanisms are different. When Na^+ concentration gradients are small as in the case of trains of bAPs in the dendrites, diffusion is not significant and removal of Na^+ is by a membrane pump [63]. The decay time constant in the dendrites of pyramidal neurons following a train of 20 bAPs was about 6 s at 23 ^oC and was reduced to 1.7 s at 33 ^oC [63] indicating that a membrane pump was controlling the removal in this time frame. When large concentration gradients are generated, as in the case of APs propagation through nodes of Ranvier or the AIS, fast removal by diffusion to internode regions or to the soma becomes the dominant mechanism responsible for the falling phase. Half recovery time of Na^+ transients in nodes is on the order of 5 ms and ouabain, a blocker of the Na^+/K^+-ATPase, has no effect on the fast recovery time (~0.3 s) of AP evoked sodium transients in the AIS [20].

In contrast to the scenarios where the falling phase negligibly overlaps with the rising phase of the Ca^{2+} transient (see previous paragraph), in other dendrites such as those of the cerebellar Purkinje neuron, the plateau is not observed. In this case, Ca^{2+} binds to Calbindin-D28k [4] and Parvalbumin [72] and the binding to Calbindin-D28k occurs within a few milliseconds or less (see the simulation of Fig.2C). This specific scenario was examined by Ait Ouares et al. [3], who showed that the dendritic Ca^{2+} current associated with a climbing fiber (CF) synaptic potential still could be estimated from the rising phase by de-convolution after analyzing the falling phase of the Ca^{2+} transient. Alternatively, the Ca^{2+}-binding processes that are responsible for the falling phase of the Ca^{2+} transient can be integrated in NEURON simulations [28] to obtain a computational estimation of the Ca^{2+} current. This approach was used by Ait Ouares et al. [2] to precisely link the dendritic Ca^{2+} current at different initial V_m, associated with CF synaptic potentials, to T-type or to P/Q-type VGCCs. Specifically, a single-compartment model comprising diverse Ca^{2+} and K^+ channels was built and parameters were optimized to match V_m and Ca^{2+} transients, obtained by combining V_m and Ca^{2+} imaging, and Ca^{2+} transients before and after the selective blockade of each individual ion channel type. In this way, it was found that T-type VGCCs are activated when the initial V_m is hyperpolarized (V_m < -75 mV) whereas P/Q-type VGCCs are activated when the initial V_m is depolarized (V_m > -55 mV). The precise characterization of the two VGCCs activated by the CF synaptic potential revealed the origin of the local supralinear Ca^{2+} signals, associated with paired parallel fiber (PF) and (CF) synaptic activity [1]. Specifically, it was found that Ca^{2+} influx triggered by activation of metabotropic glutamate receptors (mGluRs) and mediated by PF synaptic potentials, transiently saturates the endogenous buffer allowing an increase of the Ca^{2+} transient associated with the CF synaptic potential, regardless of the activated VGCC (T-type or P/Q-type). mGluR1 boosting of the T-type VGCC [27] still could be detected suggesting that the initial V_m plays an important role in the way the cell processes incoming CF and PF inputs.

Ca^{2+} and Na^+ signals in dendritic spines

The case of dendritic spines deserves particular attention since in this small compartment the ionic influx may localize over a surface < 1 μm^2. The key requirements to resolve fast ionic transients from these small areas are: (1) the use of indicators that are non-buffering over the physiological concentration ranges activated by the stimuli (either bAPs or synaptic stimulation) and (2) the use of detector systems fast enough (500 kHz or higher) to follow the ionic signals. For Ca^{2+}, very low concentrations of high affinity indicators (e.g. Oregon Green BAPTA-1, Magnesium-Green, or fluo-4) or

higher concentrations of low affinity indicators (e.g. Oregon Green BAPTA-5F, fluo4-FF) were shown to accurately follow Ca^{2+} dynamics in spines. For Na^+, the two popular indicators (SBFI and ING-2) both bind the ion with low affinity and follow spine and dendrite Na^+ changes accurately at concentrations up to 2 mM. Popular detectors of spine signals are 2-photon systems in line scan mode and fast cameras (e.g. RedShirtImaging NeuroCCD-SMQ and SciMeasure DaVinci 2K CMOS).

In dendritic spines, when the Ca^{2+} transient is evoked by a bAP, the rise time of Ca^{2+} signals was measured as <2ms using low affinity indicators and 2-photon detectors with 2 ms time resolution [67,69]. Slightly faster rise times (1.6 ms) were measured with Oregon Green BAPTA-5F and a camera with 0.5 ms time resolution [51], similar to the rise time of AP calcium signals in the dendrites [32]. In contrast to Ca^{2+}, the rise time of the bAP evoked Na^+ signal in the spine could not be determined because the signal was too weak, probably because of the low density of Na^+ channels at that location [42]. Whereas the rising phase of bAP-evoked ionic transients is governed by the kinetics of voltage-gated ion channels, the rising phase of synaptically activated Na^+ and Ca^{2+} signals in pyramidal neuron spines involve additional factors, in particular, the kinetics of AMPA and NMDA receptors and their interactions. In principle, also mGluRs contribute, but their effect on the Na^+ and Ca^{2+} spine signals appears to be insignificant when only one presynaptic spike is evoked. Synaptically activated Ca^{2+} signals in spines have been measured in many experiments (e.g. [10,11,22,29,37,55,56,79]), but rarely with low-affinity, non-buffering indicators. Synaptically activated Na^+ signals have been measured in only a few experiments, starting with the work of Rose and Konnerth [62]. Only two efforts had the time resolution to accurately follow the spine Na^+ transients [50,51]. Fig. 4 shows an example of bAP-activated and synaptically-activated Ca^{2+} and Na^+ transients in the same spine. Whereas the synaptic Ca^{2+} signal primarily is mediated by NMDA receptors, the synaptic Na^+ signal primarily is mediated by AMPA receptors. The rise times of both synaptically activated Na^+ and Ca^+ transients in spines are about 7-8 ms [51], significantly slower than the rise times of bAP evoked signals. The different slope, compared to the bAP evoked signal, is mostly a reflection of the kinetics of the synaptically activated AMPA conductance which directly determines the rise time of the Na^+ signal, and indirectly determines the rise time of the calcium signal through the removal of the Mg^{2+} block of NMDA receptors. The small contribution of VGCCs to the synaptically activated Ca^{2+} signal has about the same rise time since it is driven by the AMPA dominated excitatory postsynaptic potential [10,51]. The falling phase of bAP-evoked Ca^{2+} signals in dendritic spines is fast (10-15 ms half decay times) as measured both with two-photon systems and fast cameras [51,67]. This rapid decay is due to a combination of Ca^{2+} binding to endogenous buffers, membrane pumps, and Na^+/Ca^{2+} exchangers [71], but the exact proportion of each mechanism is not clear. Diffusion of Ca^{2+} close to the sites of entry through membrane channels is important but has not been measured accurately. The importance of removal of Ca^{2+} from spines by diffusion following synaptic activation has been difficult to determine [43,71], in part because Ca^{2+} bound to the indicator diffuses faster than free Ca^{2+} diffuses. But current experiments suggest that it is not a significant removal mechanism [74]. The falling phase of synaptically activated Ca^{2+} transients in spines is slightly slower (~26 ms) than the falling phase of bAP evoked transients [51], probably because there is some Ca^{2+} entry through the NMDA receptor after the Mg^{2+} block recovers [10], and this entry counteracts the removal process. The decay time of synaptically activated Na^+ transients in spines

ranges between 10-60 ms and is almost entirely due to diffusion of Na^+ from the spine to the dendrite. The variability in decay times probably reflects the variability of spine neck morphology, which also affects spine neck resistance. Similar to the determination of Ca^{2+} currents in axons from the derivative of the fluorescence transient, a measurement of the synaptically evoked Ca^{2+} current in spines can be calculated from the deconvolution of the evoked fluorescence transient [10,51]. In these experiments only an estimate of the time course of the current was made since the volume of a spine is much less than the volume of the axon segment used to calculate the Ca^{2+} current at that location, reducing the S/N of the measurement. Estimates of synaptically activated Na^+ currents using this method have not been made, although it seems possible. Improvement in indicators or technology (see below) may lead to better assessments of these currents.

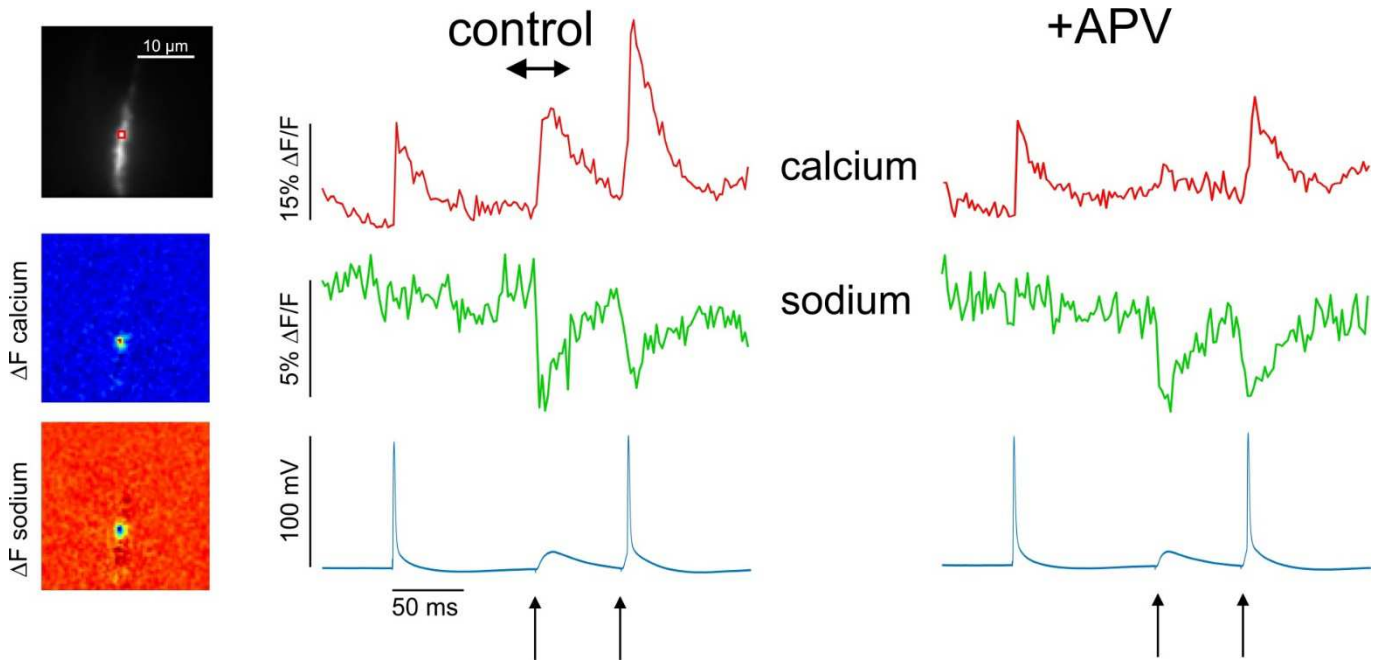

Figure 4. Comparison between Ca^{2+} and Na^+ signals in dendritic spines evoked either by a bAP or by synaptic stimulation. On the left, fluorescence image of a dendritic segment with a spine outlined in red (top) and color-scale images of Ca^{2+} and Na^+ signals(bottom) evoked by synaptic stimulation and localized on the spine. In the middle, Ca^{2+} and Na^+ signals in the dendritic spine in response to a bAP, to synaptic stimulation or to both. The Na^+ signals are shown downward because SBFI fluorescence is quenched by Na^+. On the right, responses to the same stimuli after addition of 100 µM APV to block NMDA receptors, showing that the synaptic Ca^{2+} signal, but not the Na^+ signal, was inhibited. The figure was reproduced from [51].

Discussion and perspectives

The previous paragraphs present an overview of the information that can be obtained by performing Ca^{2+} and Na^+ imaging with low-affinity indicators at high spatial and temporal resolution. While there is margin for improvement for better organic indicators, most current efforts are focused on genetically encoded indicators (GECIs). Although there have been great improvements in the speed of response and sensitivity of GECIs [80], the rise time and decay time of AP evoked transients, using these indicators, is still significantly slower than the responses with synthetic indicators. Also, there is no easy way of determining the concentration of GECIs in cells, which has a significant effect on the time course

and amplitude of fluorescence transients. Therefore, as long as the application is focused on biophysical parameters and not on circuit studies *in vivo*, synthetic indicators are preferred. Unfortunately, there has been little recent effort to improve low affinity indicators, either for Ca^{2+} or for Na^{+}, in terms of sensitivity (dynamic range) and brightness. Other technical ways for improvement can come from better detectors and light sources. The appropriate detector should have high quantum efficiency and high spatial and temporal resolution. Ideally, it should also be part of a system that rejects as much background fluorescence as possible. For instance, two-photon microscopes, because they reject out of focus light, are best at reducing background light, which is important for detecting signals from single cells in brain slices. However, individual spines located close to the slice can be often resolved by whole field illumination using CCD or CMOS cameras. For instance, the discontinued back-illuminated RedshirtImaging CCD-SMQ camera had very high quantum efficiency, low noise, and it could acquire frames at 2 kHz with 80x80 pixels resolution [50,51] or frames at 20 kHz with 4x26 pixels resolution [31,32]. The abilities of CCD technologies recently have been surpassed by CMOS cameras such as the SciMeasure DaVinci 2K that is capable of acquiring frames at 10 kHz with a 30x128 pixels resolution [18]. Currently, novel CMOS cameras with improved quantum efficiency and spatio-temporal resolution are commercially available offering significant opportunities for further advancing these types of fluorescence measurements. Notably, significant improvements in spatial resolution can be further achieved using spinning disk confocal systems [17] that reduce background light and have potentially better time resolution than 2-photon systems. An underappreciated parameter is the light source for exciting indicators. For many years arc lamps (mainly xenon) were used to activate fluorescence at the peak absorption wavelength using bandpass filters. An issue with these lamps is that they cannot be turned on and off rapidly, which requires the use of a mechanical shutter that limits the switching time to a few milliseconds. Thus, LEDs have recently replaced arc lamps in most systems because they can switch on and off in microseconds, eliminating the need for shutters, and they offer a wide selection of peak wavelengths at high intensity, which makes them adequate for most experiments. Diode lasers can also be switched on and off rapidly and high intensities can be reached in relatively cheap devices at some selected visible wavelengths. One factor, which has been found critical in some experiments [18,48], is that the narrow laser beam can be focused to a small spot, which reduces background fluorescence and lowers photodynamic damage. Future lasers, with a wider choice of wavelengths, should help the kinds of experiments discussed in this review. Finally, the techniques described in this review have been performed in a relatively low number of laboratories, sharing advanced expertise in optical techniques and electrophysiology. Up to now, this fact has limited the analysis of neuronal systems to a few cell types. Yet, an increase in the number of users would improve the detailed characterization of Ca^{2+} and Na^{+} signals in cell types that remain mainly unexplored. Another important potential future exploitation of these techniques is the study of ion channels, particularly in relation to channelopathies. As an example, rapid Ca^{2+} measurements in the AIS were used to characterize an animal model of autism caused by a point mutation of the VGNC Nav1.2, unraveling a critical change in Ca^{2+} permeability associated with this mutation [14]. In addition to this type of characterization, the optical methods presented in this review can be exploited in drug screening on brain slices since they can reveal with precision the effect of a potentially therapeutic molecule on the native system.

Declarations

Ethical Approval

Not applicable (this is an invited review)

Competing interests

The authors declare no competing interests

Authors' contributions

MC and WNR wrote the manuscript and approved it before submission

Funding

This work was supported for MC by the *Agence Nationale de la Recherche* through the Labex *Ion Channels Science and Therapeutics* (program number ANR-11-LABX-0015) and for WNR by the National Institute of Health (grant R01NS099122) and by the US-Israel Binational Science Foundation (Grant No: 2017163).

Availability of data and materials

This is an invited review that does not contain original data and materials

References

1. Ait Ouares K, Canepari M (2020) The Origin of Physiological Local mGluR1 Supralinear Ca^{2+} Signals in Cerebellar Purkinje Neurons. J Neurosci 40:1795-1809. doi: 10.1523/JNEUROSCI.2406-19.2020.
2. Ait Ouares K, Filipis L, Tzilivaki A, Poirazi P, Canepari M (2019) Two Distinct Sets of Ca2+ and K+ Channels Are Activated at Different Membrane Potentials by the Climbing Fiber Synaptic Potential in Purkinje Neuron Dendrites. J Neurosci 39:1969-1981. doi: 10.1523/JNEUROSCI.2155-18.2018.
3. Ait Ouares K, Jaafari N, Canepari M (2016) A generalised method to estimate the kineics of fast Ca(2+) currents from Ca(2+) imaging experiments. J Neurosci Methods 268:66-77. doi: 10.1016/j.jneumeth.2016.05.005.
4. Airaksinen MS, Eilers J, Garaschuk O, Thoenen H, Konnerth A, Meyer M (1997) Ataxia and altered dendritic calcium signaling in mice carrying a targeted null mutation of the calbindin D28k gene. Proc Natl Acad Sci USA 94:1488-1493. doi: 10.1073/pnas.94.4.1488.
5. Ali F, Kwan AC (2020) Interpreting in vivo calcium signals from neuronal cell bodies, axons, and dendrites: a review. Neurophotonics 7:011402. doi: 10.1117/1.NPh.7.1.011402.
6. Anselmi F, Ventalon C, Bègue A, Ogden D, Emiliani V (2011) Three-dimensional imaging and photostimulation by remote-focusing and holographic light patterning. Proc Natl Acad Sci USA 108:19504-9. doi: 10.1073/pnas.1109111108.
7. Augustine GJ (1994) Combining patch-clamp and optical methods in brain slices. J Neurosci Methods 54:63-169. doi: 10.1016/0165-0270(94)90190-2.
8. Baranauskas G, David Y, Fleidervish IA (2013) Spatial mismatch between the Na+ flux and spike initiation in axon initial segment. Proc Natl Acad Sci USA 110:4051-4056. doi: 10.1073/pnas.1215125110.
9. Bardo S, Cavazzini MG, Emptage N (2006) The role of the endoplasmic reticulum Ca2+ store in the plasticity of central neurons. Trends Pharmacol Sci. 2006 Feb;27(2):78-84. doi: 10.1016/j.tips.2005.12.008.
10. Bloodgood BL, Giessel AJ, Sabatini BL (2009) Biphasic synaptic Ca influx arising from compartmentalized electrical signals in dendritic spines. PLoS Biol 7:e1000190. doi: 10.1371/journal.pbio.1000190.
11. Bloodgood BL, Sabatini BL (2007) Nonlinear regulation of unitary synaptic signals by CaV(2.3) voltage-sensitive calcium channels located in dendritic spines. Neuron 53:249-260. doi: 10.1016/j.neuron.2006.12.017.
12. Canepari M, Mammano F (1999) Imaging neuronal calcium fluorescence at high spatio-temporal resolution. J Neurosci Methods 87:1-11. doi: 10.1016/s0165-0270(98)00127-7.
13. DiGregorio DA, Peskoff A, Vergara JL (1999) Measurement of action potential-induced presynaptic calcium domains at a cultured neuromuscular junction. J Neurosci 19:7846-7859. doi: 10.1523/JNEUROSCI.19-18-07846.1999.
14. Echevarria-Cooper DM, Hawkins NA, Misra SN, Huffman AM, Thaxton T, Thompson CH, Ben-Shalom R, Nelson AD, Lipkin AM, George AL Jr, Bender KJ, Kearney JA (2022) Cellular and

behavioral effects of altered NaV1.2 sodium channel ion permeability in Scn2aK1422E mice. Hum Mol Genet 31:2964-2988. doi: 10.1093/hmg/ddac087.

15. Faas GC, Schwaller B, Vergara JL, Mody I (2007) Resolving the fast kinetics of cooperative binding: Ca2+ buffering by calretinin. PLoS Biol 5:e311. doi: 10.1371/journal.pbio.0050311.
16. Fierro L, Llano I (1996) High endogenous calcium buffering in Purkinje cells from rat cerebellar slices. J Physiol 496:617-625. doi: 10.1113/jphysiol.1996.sp021713.
17. Filipis L, Ait Ouares K, Moreau P, Tanese D, Zampini V, Latini A, Bleau C, Bleau C, Graham J, Canepari M (2018) A novel multisite confocal system for rapid Ca^{2+} imaging from submicron structures in brain slices. J Biophotonics:11(3). doi: 10.1002/jbio.201700197.
18. Filipis L, Canepari M (2021) Optical measurement of physiological sodium currents in the axon initial segment. J Physiol 599:49-66. doi: 10.1113/JP280554.
19. Filipis, L, Blömer LA, Montnach J, De Waard M, Canepari, M (2023) Nav1.2 and BK channels interaction shapes the action potential in the axon initial segment. J Physiol 601:1957-1979. doi: 10.1113/JP283801.
20. Fleidervish IA, Lasser-Ross N, Gutnick MJ, Ross WN (2010) Na+ imaging reveals little difference in action potential-evoked Na+ influx between axon and soma. Nat Neurosci 13:852-860. doi: 10.1038/nn.2574.
21. Grienberger C, Konnerth A (2012) Imaging calcium in neurons. Neuron 73:862-885. doi: 10.1016/j.neuron.2012.02.011.
22. Grunditz A, Holbro N, Tian L, Zuo Y, Oertner TG (2008) Spine neck plasticity controls postsynaptic calcium signals through electrical compartmentalization. J Neurosci 28:13457-13466. doi: 10.1523/JNEUROSCI.2702-08.2008.
23. Guy HR, Conti F (1990) Pursuing the structure and function of voltage-gated channels. Trends Neurosci 13:201-206. doi: 10.1016/0166-2236(90)90160-c.
24. Hanemaaijer NA, Popovic MA, Wilders X, Grasman S, Pavón Arocas O, Kole MH (2020) Ca^{2+} entry through Na_V channels generates submillisecond axonal Ca^{2+} signaling. Elife 9:e54566. doi: 10.7554/eLife.54566.
25. Helmchen F, Imoto K, Sakmann B (1996) Ca2+ buffering and action potential-evoked Ca2+ signaling in dendrites of pyramidal neurons. Biophys J 70:1069-1081. doi: 10.1016/S0006-3495(96)79653-4.
26. Higley MJ, Sabatini BL (2008) Calcium signaling in dendrites and spines: practical and functional considerations. Neuron 59:902-913. doi: 10.1016/j.neuron.2008.08.020.
27. Hildebrand ME, Isope P, Miyazaki T, Nakaya T, Garcia E, Feltz A, Schneider T, Hescheler J, Kano, M, Sakimura K, Watanabe M, Dieudonné S, Snutch TP (2009) Functional coupling between mGluR1 and Cav3.1 T-type calcium channels contributes to parallel fiber-induced fast calcium signaling within Purkinje cell dendritic spines. J Neurosci 29 :9668-9682. doi: 10.1523/JNEUROSCI.0362-09.2009.
28. Hines ML, Carnevale NT (1997) The NEURON simulation environment. Neural Comput 9:1179-1209. doi: 10.1162/neco.1997.9.6.1179.

29. Holbro N, Grunditz A, Wiegert JS, Oertner TG (2010) AMPA receptors gate spine Ca(2+) transients and spike-timing-dependent potentiation. Proc Natl Acad Sci USA 107 :15975-15980. doi: 10.1073/pnas.1004562107.
30. Hsieh LS, Levine ES (2013) Cannabinoid modulation of backpropagating action potential-induced calcium transients in layer 2/3 pyramidal neurons. Cereb Cortex 23:1731-1741. doi: 10.1093/cercor/bhs168.
31. Jaafari N, Canepari M (2016) Functional coupling of diverse voltage-gated Ca(2+) channels underlies high fidelity of fast dendritic Ca(2+) signals during burst firing. J Physiol 594:967-983. doi: 10.1113/JP271830.
32. Jaafari N, De Waard M, Canepari M (2014) Imaging Fast Calcium Currents beyond the Limitations of Electrode Techniques. Biophys J 107:1280-1288. doi: 10.1016/j.bpj.2014.07.059.
33. Jaafari N, Marret E, Canepari M (2015) Using simultaneous voltage and calcium imaging to study fast Ca2+ channels. Neurophotonics 2:021010. doi: 10.1117/1.NPh.2.2.021010.
34. Kao JP, Tsien RY (1988) Ca2+ binding kinetics of fura-2 and azo-1 from temperature-jump relaxation measurements. Biophys J 53:635-639. doi: 10.1016/S0006-3495(88)83142-4.
35. Kaplan JH (2002) Biochemistry of Na,K-ATPase. Annu Rev Biochem 71:511-535. doi: 10.1146/annurev.biochem.71.102201.141218.
36. Katz E, Stoler O, Scheller A, Khrapunsky Y, Goebbels S, Kirchhoff F, Gutnick MJ, Wolf F, Fleidervish IA (2018) Role of sodium channel subtype in action potential generation by neocortical pyramidal neurons. Proc Natl Acad Sci USA 115:E7184-E7192. doi: 10.1073/pnas.1720493115.
37. Kovalchuk Y, Eilers J, Lisman J, Konnerth A (2000) NMDA receptor-mediated subthreshold Ca(2+) signals in spines of hippocampal neurons. J Neurosci 20:1791-1799. doi: 10.1523/JNEUROSCI.20-05-01791.2000.
38. Kushmerick MJ, Podolsky RJ (1969) Ionic mobility in muscle cells. Science 166:1297-1298. doi: 10.1126/science.166.3910.1297.
39. Lee SH, Schwaller B, Neher E (2000) Kinetics of Ca2+ binding to parvalbumin in bovine chromaffin cells: implications for [Ca2+] transients of neuronal dendrites. J Physiol 525:419-432. doi: 10.1111/j.1469-7793.2000.t01-2-00419.x.
40. Lipkin AM, Cunniff MM, Spratt PWE, Lemke SM, Bender KJ (2021) Functional Microstructure of CaV-Mediated Calcium Signaling in the Axon Initial Segment. J Neurosci 41:3764-3776. doi: 10.1523/JNEUROSCI.2843-20.2021.
41. Looger LL, Griesbeck O (2012) Genetically encoded neural activity indicators. Curr Opin Neurobiol 22:18-23. doi: 10.1016/j.conb.2011.10.024.
42. Lorincz A, Nusser Z (2010) Molecular identity of dendritic voltage-gated sodium channels. Science 328:906-909. doi: 10.1126/science.1187958.
43. Majewska A, Brown E, Ross J, Yuste R (2000) Mechanisms of calcium decay kinetics in hippocampal spines: role of spine calcium pumps and calcium diffusion through the spine neck in biochemical compartmentalization. J Neurosci 20:1722-1734. doi: 10.1523/JNEUROSCI.20-05-01722.2000.

44. Mata AM, Sepúlveda MR (2005) Calcium pumps in the central nervous system. Brain Res Brain Res Rev 49:398-405. doi: 10.1016/j.brainresrev.2004.11.004.
45. Matthews EA, Dietrich D (2015) Buffer mobility and the regulation of neuronal calcium domains. Front Cell Neurosci 9:48. doi: 10.3389/fncel.2015.00048.
46. Minta A, Tsien RY (1989) Fluorescent indicators for cytosolic sodium. J Biol Chem 264:19449-19457.
47. Miyakawa H, Lev-Ram V, Lasser-Ross N, Ross WN (1992) Calcium transients evoked by climbing fiber and parallel fiber synaptic inputs in guinea pig cerebellar Purkinje neurons. J Neurophysiol 68:1178-11789. doi: 10.1152/jn.1992.68.4.1178.
48. Miyazaki K, Lisman JE, Ross W (2019) Improvements in Simultaneous Sodium and Calcium Imaging. Front Cell Neurosci 12:514. doi: 10.3389/fncel.2018.00514.
49. Miyazaki K, Ross WN (2015) Simultaneous Sodium and Calcium Imaging from Dendrites and Axons. eNeuro 2, ENEURO.0092-15.2015. doi: 10.1523/ENEURO.0092-15.2015.
50. Miyazaki K, Ross WN (2017) Sodium Dynamics in Pyramidal Neuron Dendritic Spines: Synaptically Evoked Entry Predominantly through AMPA Receptors and Removal by Diffusion. J Neurosci 37:9964-9976. doi: 10.1523/JNEUROSCI.1758-17.2017.
51. Miyazaki K, Ross WN (2022) Fast synaptically activated calcium and sodium kinetics in hippocampal pyramidal neuron dendritic spines. eNeuro 9:ENEURO.0396-22.2022. doi: 10.1523/ENEURO.0396-22.2022.
52. Mondragão MA, Schmidt H, Kleinhans C, Langer J, Kafitz KW, Rose CR (2016) Extrusion versus diffusion: mechanisms for recovery from sodium loads in mouse CA1 pyramidal neurons. J Physiol 594:5507-5527. doi: 10.1113/JP272431.
53. Murphy JG, Gutzmann JJ, Lin L, Hu J, Petralia RS, Wang YX, Hoffman DA (2022) R-type voltage-gated Ca^{2+} channels mediate A-type K^{+} current regulation of synaptic input in hippocampal dendrites. Cell Rep 38:110264. doi: 10.1016/j.celrep.2021.110264.
54. Nägerl UV, Novo D, Mody I, Vergara JL (2000) Binding kinetics of calbindin-D(28k) determined by flash photolysis of caged Ca(2+). Biophys J 79:3009-3018. doi: 10.1016/S0006-3495(00)76537-4.
55. Nevian T, Sakmann B (2006) Spine Ca2+ signaling in spike-timing-dependent plasticity. J Neurosci 26:11001-11013. doi: 10.1523/JNEUROSCI.1749-06.2006.
56. Noguchi J, Matsuzaki M, Ellis-Davies GC, Kasai H (2005) Spine-neck geometry determines NMDA receptor-dependent Ca2+ signaling in dendrites. Neuron 46:609-622. doi: 10.1016/j.neuron.2005.03.015.
57. Ogden D, Khodakhah K, Carter T, Thomas M, Capiod T (1995) Analogue computation of transient changes of intracellular free Ca2+ concentration with the low affinity Ca2+ indicator furaptra during whole-cell patch-clamp recording. Pflugers Arch 429:587-591. doi: 10.1007/BF00704165.
58. Pankratov Y, Lalo U (2014) Calcium permeability of ligand-gated Ca2+ channels. Eur J Pharmacol 739:60-73. doi: 10.1016/j.ejphar.2013.11.017.

59. Paredes RM, Etzler JC, Watts LT, Zheng W, Lechleiter JD (2008) Chemical calcium indicators. Methods 46:143-151. doi: 10.1016/j.ymeth.2008.09.025.
60. Ramirez JE, Stell BM (2016) Calcium Imaging Reveals Coordinated Simple Spike Pauses in Populations of Cerebellar Purkinje Cells. Cell Rep 17:3125-3132. doi: 10.1016/j.celrep.2016.11.075.
61. Roder P, Hille C (2014). ANG-2 for quantitative Na+ determination in living cells by time-resolved fluorescence microscopy. Photochem Photobiol Sci 13:1699-1710. doi: 10.1039/c4pp00061g.
62. Rose CR, Konnerth A (2001) NMDA receptor-mediated Na+ signals in spines and dendrites. J Neurosci 21:4207-4214. doi: 10.1523/JNEUROSCI.21-12-04207.2001.
63. Rose CR, Kovalchuk Y, Eilers J, Konnerth A (1999) Two-photon Na+ imaging in spines and fine dendrites of central neurons. Pflugers Arch 439:201-207. doi: 10.1007/s004249900123.
64. Ross WN, Miyazaki K, Popovic MA, Zecevic D (2015) Imaging with organic indicators and high-speed charge-coupled device cameras in neurons: some applications where these classic techniques have advantages. Neurophotonics 2:021005. doi: 10.1117/1.NPh.2.2.021005.
65. Rossi B, Ogden D, Llano I, Tan YP, Marty A, Collin T (2012) Current and calcium responses to local activation of axonal NMDA receptors in developing cerebellar molecular layer interneurons. PLoS One 7:e39983. doi: 10.1371/journal.pone.0039983.
66. Sabatini BL, Maravall M, Svoboda K (2001) Ca(2+) signaling in dendritic spines. Curr Opin Neurobiol 11:349-356. doi: 10.1016/s0959-4388(00)00218-x.
67. Sabatini BL, Oertner TG, Svoboda K (2002) The life cycle of Ca^{2+} ions in dendritic spines. Neuron 33:439-452. doi: 10.1016/s0896-6273(02)00573-1.
68. Sabatini BL, Regehr WG (1998) Optical measurement of presynaptic calcium currents. Biophys J 74:1549-1563. doi: 10.1016/S0006-3495(98)77867-1.
69. Sabatini BL, Svoboda K (2000) Analysis of calcium channels in single spines using optical fluctuation analysis. Nature 408:589-593. doi: 10.1038/35046076.
70. Sakmann B, Neher E (1984) Patch clamp techniques for studying ionic channels in excitable membranes. Annu. Rev. Physiol 46:455–472. doi: 10.1146/annurev.ph.46.030184.002323.
71. Scheuss V, Yasuda R, Sobczyk A, Svoboda K (2006) Nonlinear [Ca2+] signaling in dendrites and spines caused by activity-dependent depression of Ca2+ extrusion. J Neurosci 26:8183-8194. doi: 10.1523/JNEUROSCI.1962-06.2006.
72. Schmidt H, Stiefel KM, Racay P, Schwaller B, Eilers J (2003) Mutational analysis of dendritic Ca2+ kinetics in rodent Purkinje cells: role of parvalbumin and calbindin D28k. J Physiol 551:13-32. doi: 10.1113/jphysiol.2002.035824.
73. Shvartsman A, Kotler O, Stoler O, Khrapunsky Y, Melamed I, Fleidervish IA (2021) Subcellular distribution of persistent sodium conductance in cortical pyramidal neurons. J Neurosci 41:6190-6201. doi: 10.1523/JNEUROSCI.2989-20.2021.
74. Sobczyk A, Scheuss V, Svoboda K (2005) NMDA receptor subunit-dependent [Ca2+] signaling in individual hippocampal dendritic spines. J Neurosci 25:6037-6046. doi: 10.1523/JNEUROSCI.1221-05.2005.

75. Strobel C, Sullivan RKP, Stratton P, Sah P (2017) Calcium signalling in medial intercalated cell dendrites and spines. J Physiol 2017 595:5653-5669. doi: 10.1113/JP274261.
76. Stuart GJ, Sakmann B (1994) Active propagation of somatic action potentials into neocortical pyramidal cell dendrites. Nature 367:69-72. doi: 10.1038/367069a0.
77. Vennekens R, Menigoz A, Nilius B (2012) TRPs in the Brain. Rev Physiol Biochem Pharmacol 2012;163:27-64. doi: 10.1007/112_2012_8.
78. Yu FH, Catterall WA (2004) The VGL-chanome: a protein superfamily specialized for electrical signaling and ionic homeostasis. Sci STKE 2004(253):re15. doi: 10.1126/stke.2532004re15.
79. Yuste R, Majewska A, Cash SS, Denk, W (1999) Mechanisms of calcium influx into hippocampal spines: heterogeneity among spines, coincidence detection by NMDA receptors, and optical quantal analysis. J Neurosci 19:1976-1987. doi: 10.1523/JNEUROSCI.19-06-01976.1999.
80. Zhang Y, Looger LL (2023) Fast and sensitive GCaMP calcium indicators for neuronal imaging. J Physiol doi: 10.1113/JP283832.